

# From Spurious to Causal: Low-rank Orthogonal Subspace Intervention for Generalizable Face Forgery Detection

Chi Wang<sup>1\*</sup>, Xinjue Hu<sup>1\*</sup>, Boyu Wang<sup>1</sup>, Ziwen He<sup>1</sup>, Zhangjie Fu<sup>1†</sup>

<sup>1</sup>School of Computer Science, Nanjing University of Information Science and Technology

202412200715@nuist.edu.cn, xinjueh@126.com, 202412200714@nuist.edu.cn

ziwen.he@nuist.edu.cn, fzj@nuist.edu.cn

## Abstract

The generalization problem remains a critical challenge in face forgery detection. Some researches have discovered that “a backdoor path” in the representations from forgery-irrelevant information to labels induces biased learning, thereby hindering the generalization. In this paper, these forgery-irrelevant information are collectively termed spurious correlations factors. Previous methods predominantly focused on identifying concrete, specific spurious correlation and designing corresponding solutions to address them. However, spurious correlations arise from unobservable confounding factors, making it impractical to identify and address each one individually. To address this, we propose an intervention paradigm for representation space. Instead of tracking and blocking various instance-level spurious correlation one by one, we uniformly model them as a low-rank subspace and intervene in them. Specifically, we decompose spurious correlation features into a low-rank subspace via orthogonal low-rank projection, subsequently removing this subspace from the original representation and training its orthogonal complement to capture forgery-related features. This low-rank projection removal effectively eliminates spurious correlation factors, ensuring that classification decision is based on authentic forgery cues. With only **0.43M** trainable parameters, our method achieves state-of-the-art performance across several benchmarks, demonstrating excellent robustness and generalization.

## 1. Introduction

Thanks to the rapid development of artificial intelligence, face forgery techniques<sup>1</sup> has made it possible to easily ma-

\*Equal contribution.

†Corresponding authors.

<sup>1</sup>Face forgery strictly refers to techniques that manipulate local facial content, e.g., lip motion editing, central-face swapping, etc. Full-image

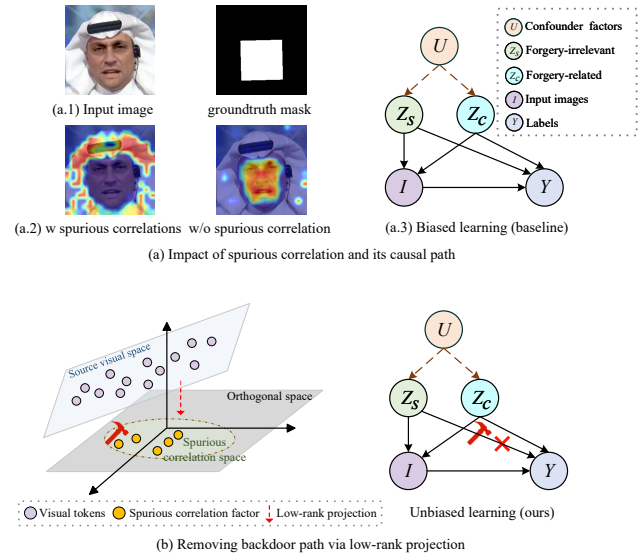


Figure 1. (a) An example of the impact of spurious correlations on Vanilla CLIP [38]. A backdoor path exists from forgery-irrelevant information (e.g. background style, identity information) to labels. (b) Causal intervention. We propose orthogonal low-rank projection to remove the spurious correlation subspace, disrupting the backdoor path.

nipulate a real face (e.g., face swapping [19], expression modification [42]). In recent years, facial manipulation has attracted considerable attention due to its convenience and has been widely used in film and television production. However, if this technology is used maliciously (e.g., digital fraud and spread of fake news), it will undoubtedly pose a significant threat to social security and media credibility [51, 53]. Therefore, there is an urgent need to develop a generalizable and robust face forgery detector.

Early paradigms typically define face forgery detection as a standard “real vs fake” binary classification problem. They utilize deep neural networks to extract facial features,

synthesis via GAN/Diffusion is out of scope.

which are then fed into a classifier to obtain the probability of “fake” for classification. In addition, some works have attempted to utilize different auxiliary information to mine forgery clues, including frequency signals [32, 37], biological signals [12, 36], spatiotemporal clues [14], and so on. Although they achieve good results on the training set, their performance drops greatly when facing unknown face manipulation methods. A common explanation [41] is: these methods often fall into local optimal solutions and overfit specific forgery patterns in training data, which hinders their performance in cross-dataset evaluation.

A practical remedy is to leverage pre-trained knowledge from visual foundation models (VFM) to expand the feature space and mitigate overfitting [47]. CLIP [38], a representative vision–language model, demonstrates strong zero-shot transfer on downstream tasks. Motivated by this, recent studies have adapted CLIP for face forgery detection using two main routes: adapter-based structured fine-tuning [6, 14, 18] and prompt-based conditional alignment [24, 52]. Empirical results show that pre-training knowledge helps capture forgery cues and yields notable improvements. However, CLIP’s semantic space is large and structurally complex. Forgery-related knowledge and forgery-irrelevant factors are often entangled within the same representation. When relying solely on external adapters or prompts, there is no explicit mechanism to decompose and constrain these two components inside the representation space. As a result, optimization can absorb task-irrelevant statistical patterns, which increases sensitivity to domain shifts and reduces cross-distribution stability. Guided by these observations, we pose the core problem as follows: How can CLIP’s internal representations be adjusted during training so that the model focuses on modeling forgery cues while suppressing forgery-irrelevant factors?

This paper explores this issue from a causal learning perspective. Visual representations contain both causal factors related to forgery and non-causal factors unrelated to forgery. When all parameters are frozen and only one trainable classification head is added, Vanilla CLIP [38] tends to treat non-causal factors (e.g., background, identity, and domain differences) as discriminative cues, thereby degrading detection performance (see Figure 1 (a.2)). From a causal perspective, these forgery-irrelevant factors easily form the backdoor path to labels, leading CLIP to shortcut learning and deviate from the correct causal path from forgery traces to labels (see Figure 1 (a.3)). A straightforward solution is to design suppression strategies for specific spurious correlation. However, spurious correlations are complex and variable, often arising from unobservable confounding factors. Such targeted approaches struggle to completely eliminate backdoor paths at the representation level.

To address this issue, we propose a novel method called **SeLop** (Spurious correlation elimination via Low-rank

orthogonal projection for face forgery detection). SeLop performs a subspace-level unified intervention in CLIP’s visual representation space and constrains the decision evidence to align with forgery cues. The key idea of SeLop is to regard all spurious correlations factors as a compressible low-rank whole, as shown in Figure 1 (b). Within the same subspace, we perform holistic modeling and constraint on these factors and enforce orthogonal separation from forgery-related cues. This avoids per-case enumeration and local patching, and achieves overall removal of spurious correlations in the representation space. Specifically, we define a trainable basis matrix and perform QR decomposition on it to obtain the required low-rank orthogonal space. We then project the original CLIP visual space into the low-rank orthogonal space to obtain the spurious correlation subspace. Finally, we remove this subspace from the visual representation, allowing the true causal factors to be concentrated in the orthogonal complement space. Through end-to-end training with a very low parameter count of **0.43M**, the model identifies spurious correlation factors and knows what should be removed in order to learn causal discriminant factors. The explicit orthogonality also maximizes the retention of CLIP’s rich pre-training knowledge while learning forgery-related features.

Overall, the main contributions of this paper are as follows:

1. In this paper, we approach spurious correlations from a new perspective: rather than discovering a specific backdoor path, we consider the backdoor path relationships caused by spurious correlations as a whole and intervene accordingly.
2. We effectively intervene in CLIP’s original visual space through orthogonal low-rank removal with minimal parameters, enabling CLIP to learn to rely on the correct causal path for classification decisions.
3. Extensive experiments on several standard benchmarks demonstrate the superior generalization and robustness of our method. In particular, with only 0.43M trainable parameters, our method achieves state-of-the-art performance.

## 2. Related Work

### 2.1. Face Forgery Detection

The rapid advancement of artificial intelligence technologies has spurred diversification in facial forgery techniques. Presently, improving generalizability of detection models remains a challenging issue in face forgery detection tasks. Previous work has focused on meticulously designing deep neural networks to learn “specific and fake patterns”, including biological signals (e.g., lip movement [12], gaze angle [36]), frequency anomalies (e.g., F2Trans [32], F3Net [37]), and identity disentanglement (e.g., CADD [10]).

However, due to the limited forgery patterns in training datasets, models often overfit and fail to generalize to unknown forgery techniques. To mitigate overfitting, [22, 41] proposed a pseudo-fake face generation strategy. Training models on custom datasets improved generalization to some extent. However, expecting models to learn all forgery patterns on custom data remains impractical.

With the advent of large language models (LLMs), pre-trained visual foundation models (e.g., CLIP [38]) on massive data have demonstrated strong generalization across downstream tasks. Recent research has explored adapting CLIP for face forgery detection. UDD [11] designed a shuffle branch and a mix branch to break position and content biases of the CLIP. GM-DF [20] proposes a domain-aware hybrid expert modelling approach within a meta-learning framework, achieving generalized multi-scenario detection. RepDFD [24] injects perturbations into input images to re-program pre-trained VLM models. Forensic-Adapter [6] introduces an adapter specifically to learn blending boundaries, achieving excellent generalization through interaction between CLIP and the adapter. Effort [47] employs Singular Value Decomposition (SVD) to decouple the feature space of attention, preserving pre-trained knowledge while learning forgery patterns.

## 2.2. Causal Learning

In recent years, causal learning has attracted significant attention in the field of computer vision. Mitigating spurious correlations through causal intervention has proven a promising approach to improving cross-domain generalization [50]. Recently, some researchers have introduced causal learning into face forgery detection. UDD [11] identified position and content biases in CLIP [38], designing shuffling and mixing branches to break inherent biases and achieve great generalization.

However, as spurious correlations arise from unobserved confounding factors, accurately identifying and intervening in all spurious correlations is impractical. Therefore, this paper proposes to intervene in the visual representations of pre-trained foundation models (e.g., CLIP) to mitigate spurious correlations.

## 3. Problem Formulation

Face forgery detection is typically modeled as a binary classification problem, wherein the task involves determining whether a given face image is authentic or forged. Given a face image  $I$  and a label  $Y \in \{0, 1\}$  (0 = real, 1 = fake), our goal is to learn a classifier that minimizes the distance between the predicted label and the ground-truth label, which can be formalized as:

$$\min_{\phi, f} \mathbb{E}[\ell(f(\phi(I)), Y)], \quad (1)$$

where  $\phi(I)$  denotes visual representations of face image  $I$ ,  $f$  denotes a classifier, and  $\ell$  denotes the loss function in the training process. The expectation  $\mathbb{E}$  is taken over the data distribution.

In this paper, we formulate the problem of face forgery detection from a novel perspective of causal learning. Following [11], we utilize Structural Causal Model (SCM) [35] to define the relevant variables and factors, as shown in Figure 1. Let  $U$  denote unobserved latent *confounders*,  $Z_s$  denote *spurious correlation* factors (e.g., identity, background), and  $Z_c$  denote *causal* factors induced by manipulations (e.g., forgery traces). In this SCM, the real causal path  $U \rightarrow Z_c \rightarrow Y$  carries forgery-related causal factors, whereas  $U \rightarrow Z_s \rightarrow Y$  constitutes a backdoor path that induces spurious correlations in training process.

However, under ideal circumstance, the classifier should rely solely on forgery-related features to determine authenticity, and be invariant to interference of forgery-irrelevant factors  $Z_s$ . Since  $Z_s$  and  $Z_c$  are unobserved during training, we impose these desiderata at the representation level. Given an input face image  $I$ , we write its representation as  $R = \phi(I) = h(Z_s, Z_c, \varepsilon)$ . For brevity, the encoder  $h(\cdot)$  mixes  $Z_s$  and  $Z_c$  into the representation  $R$ . We seek a representation that (i) preserves causal factor  $Z_c$  for predicting  $Y$ , and (ii) blocks the backdoor path:

$$\underbrace{I(Y; R)}_{\text{causal sufficiency}} \geq \kappa \quad \text{and} \quad \underbrace{Y \perp\!\!\!\perp Z_s \mid R}_{\text{backdoor blocking / invariance}} \quad (2)$$

where  $I(\cdot)$  denotes mutual information,  $\kappa$  is a threshold. Intuitively, the learned representation should retain enough information about the forgery-related factor  $Z_c$  that determines  $Y$ , while being insensitive to spurious factors  $Z_s$  or discard them. In the next section, we describe a transformation on  $\phi(I)$  that achieves these causal desiderata.

## 4. Methodology

### 4.1. Theoretical Analysis

To decouple spurious correlation factors from visual representations at the representation-level, we first consider separability of visual representations. According to previous section, visual representations  $R = h(Z_s, Z_c, \varepsilon)$ .

A first-order expansion yields:

$$\Delta R \approx J_s \Delta z_s + J_c \Delta z_c, \quad (3)$$

where  $J_s = \partial h / \partial z_s \in \mathbb{R}^{D \times m_s}$  and  $J_c = \partial h / \partial z_c \in \mathbb{R}^{D \times m_c}$ . We assume that  $\Delta z_s$  and  $\Delta z_c$  are independent and zero-mean, then the cross term vanishes and  $R$  admits an additive form. The equation is expressed as:

$$R \approx S + N + \xi, \quad \text{Cov}(S, N) \approx 0, \quad (4)$$

where  $S$  approximates forgery-related representations, while  $N$  denotes representations of spurious correlation.

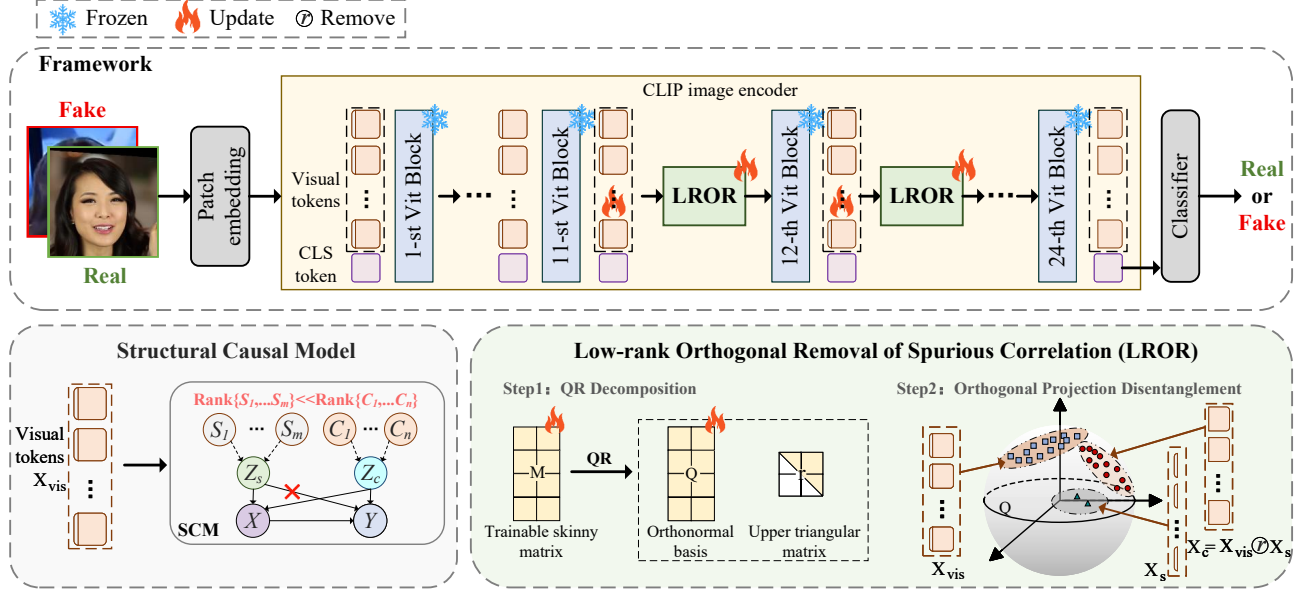


Figure 2. **Pipeline of the proposed method SeLop.** Based on the Structural Causal Model, we propose Low-rank Orthogonal Removal of Spurious Correlation (LROR) to mitigate influence of forgery-irrelevant factors  $X_s$ , which aims to break the backdoor path from spurious correlations to labels. See text for details.

This decomposition relies on the assumption that the causal and spurious components are locally separable and approximately independent, which facilitates analytical tractability. Details are provided in supplementary material Sec.2. Moreover, (3) implies that spurious correlation variation lies in the column space of  $J_s$ :

$$\text{rank}(\text{Cov}(N)) = \text{rank}(J_s \Sigma_s J_s^\top) \leq m_s \ll D. \quad (5)$$

where Cov is Covariance. If spurious correlation is driven by a discrete domain variable  $G \in \{1, \dots, K\}$ , the covariance admits an ANOVA decomposition  $\Sigma_R = \mathbb{E}[\Sigma_{R|G}] + \sum_{k=1}^K \pi_k (\mu_k - \mu)(\mu_k - \mu)^\top$ , whose between-domain term has rank at most  $K-1$ . Hence the spurious correlation component concentrates in a low-dimensional subspace  $\mathcal{U}$  with effective rank  $r \leq m_s + (K-1) \ll D$ :

$$R \approx S + N + \xi, \quad \text{dim}(\mathcal{U}) = r \ll D. \quad (6)$$

Equations (4)–(6) summarize theoretical analysis we rely on: **the causal and spurious factors are approximately separable in the visual representation, and the spurious component is low-rank compressible**.

## 4.2. Low-rank Orthogonal Removal of Spurious Correlation

According to the heuristic analysis of Sec 4.1, we propose an orthogonal low-rank projection to intervene in the visual space of CLIP. Our goal is to enable the model to adaptively and correctly remove the influence of spurious correlation features in the visual representation through training,

and utilize the forgery-related features to make classification decisions.

In order to retain CLIP’s rich pre-training knowledge to the maximum extent, we only apply the projection intervention in the middle and deep layers of the CLIP to estimate a spurious correlation subspace  $\mathcal{U}$  (see Figure 2).

Specifically, let  $X \in \mathbb{R}^{B \times (1+N_p) \times D}$  denote CLIP tokens in every transformer layer. Note that CLIP tokens  $X$  comprise visual tokens  $X_{\text{vis}} \in \mathbb{R}^{B \times N_p \times D}$  and [CLS] token  $X_{[\text{CLS}]} \in \mathbb{R}^{B \times 1 \times D}$ , denoted as  $X = [X_{\text{vis}}, X_{[\text{CLS}]}]$ .  $B$  denote batchsize of the training process,  $N_p$  denote number of visual tokens and  $D$  denote hidden dimension of CLIP tokens. Consider all visual tokens as a visual space  $X_{\text{vis}} \in \mathbb{R}^{N_p \times D}$ , which is equivalent to the visual representation  $\phi(I)$  that we discussed earlier. Intervention at each layer is implemented with a trainable skinny matrix  $M \in \mathbb{R}^{D \times r}$ . Firstly, we perform QR decomposition on  $M$  to obtain an orthonormal basis  $Q \in \mathbb{R}^{D \times r}$ ,  $r \ll D$ :

$$Q, r = QR(M) \quad (7)$$

where  $Q^\top Q = I_r$ ,  $Q$  is a column-orthogonal matrix and  $r$  is an upper triangular matrix. Then, we decompose visual tokens into a low-rank compression subspaces  $\mathcal{U}$ :

$$\mathcal{U} = X_s = X_{\text{vis}} Q Q^\top \quad (8)$$

Due to the approximate separability and low-rank compressibility (see equation 6), forgery-irrelevant features are projected into this low-rank subspace through training. The causal factors associated with artifacts have been learned

within orthogonal complement space. Specifically, its orthogonal complement space is:

$$X_c = X_{vis} - \mathcal{U} \quad (9)$$

Finally, we concat  $X_c$  and  $X_{[CLS]}$  to form a new token stream  $[X_c, X_{[CLS]}]$  and feed it to the next transformer layer. During training, we only optimize  $\mathbf{Q}$ , and the final fully-connected layer while keeping the parameters of all transformer block fixed. This implementation ensures the preservation of pre-trained knowledge of CLIP while reducing the introduction of extraneous noise. Formally, our model learns  $\mathbf{Q}$  to push  $X_{vis}\mathbf{Q}\mathbf{Q}^\top$  to align with spurious variation from  $Z_s$  and removes it, preserving causal evidence from  $Z_c$  ( $U \rightarrow Z_c \rightarrow Y$ ) and blocking the backdoor  $U \rightarrow Z_s \rightarrow Y$ .

**Objective.** After intervening in the visual space of CLIP, our goal can be formulated as:

$$\begin{aligned} \min_{\phi, f, \mathbf{Q}} \mathbb{E}_{(X, Y)} & \left[ \ell(f(\phi(I) P_\perp), Y) \right] \\ \text{s.t. } P_\perp &= I - \mathbf{Q}\mathbf{Q}^\top, \mathbf{Q}^\top \mathbf{Q} = I_r \end{aligned} \quad (10)$$

In the training phase, the main objective function is a Cross-entropy loss applied on  $X_{[CLS]}$  in the last layer of CLIP.

### 4.3. How to remove spurious correlation subspaces and why our method works

We define spurious correlation as representation directions that correlate with the label via forgery-irrelevant information (e.g., background, identity) rather than forgery traces. Formally, letting the representation be  $R = h(Z_s, Z_c, \varepsilon)$  and taking a first-order local expansion around a reference point yields  $R \approx J_s \Delta z_s + J_c \Delta z_c$ , where the variation aligned with  $Z_s$  (the spurious component  $N := J_s \Delta z_s$ ) is considered to be low-rank and approximately additive with the forgery-related component  $S := J_c \Delta z_c$ . We model the spurious correlation subspace by a column-orthonormal basis  $Q \in \mathbb{R}^{D \times r}$  with  $r \ll D$ , obtained by orthogonalizing a slim learnable matrix  $B$  via QR decomposition to get  $Q$ , which induces the projector  $P = Q\mathbf{Q}^\top$  and its orthogonal complement  $P_\perp = I - P$ . At both training and inference, we remove spurious correlations by applying  $P_\perp$  to token features. Under the row-wise convention for features  $X \in \mathbb{R}^{N \times D}$ , we compute  $X_c = X P_\perp = X(I - P)$ , thus preserving forgery-related signal while suppressing nuisance directions. The orthogonal basis  $Q$  is learned end-to-end purely from the cross-entropy loss: if  $Q$  captures shortcuts, projecting them out improves generalization; if it mistakenly captures causal factors, the loss penalizes it and drives  $Q$  away. This yields a precise mechanism to excise spurious correlation subspaces without any explicit supervision of  $Z_s$  or  $Z_c$ .

## 5. Experiments

### 5.1. Experimental Settings

**Datasets.** To comprehensively and fairly evaluate the model’s generalization ability, we follow the DeepFakeBench protocol [45] and utilize six publicly available datasets: FaceForensics++ (FF++) [40], Celeb-DF (CDF-v1 and CDF-v2) [23], Deepfake Detection Challenge dataset (DFDC) [9], DeepFake Detection Challenge Preview (DFDCP) [8], and Deepfakedetection (DFD) [7]. Our method is trained on c23 compression version of FF++ and tested on other datasets. In this paper, following the latest method [47, 49], we adopt two widely used and standard protocols for evaluation: **Protocol-1**: cross-dataset evaluation, **Protocol-2**: cross-manipulation evaluation within the FF++ data domain. For **Protocol-1**, all methods are trained on FF++ c23 training set and evaluated on other deepfake datasets. For **Protocol-2**, we evaluate the models on the latest deepfake dataset DF40 [48], which includes four types of forgery methods: face swapping, face reenactment, whole face synthesis, and face editing. Moreover, these forged faces are generated within the FF++ domain, ensuring the manipulation methods different while the data domains remain unchanged. For specific experimental details, refer to the supplementary material Sec.4.

**Evaluation Metrics.** Following the most existing work [6, 11, 46], we utilize area under receiver operating characteristic curve (AUC) scores for generalization evaluation in experiments. In our paper, we report results for both frame-level AUC and video-level AUC. Frame-level AUC is calculated based on the predicted scores of face frames. In line with these methods, video-level AUC is computed by averaging the model’s outputs across frames of a video.

### 5.2. Comparison with State-of-the-art Methods

In this section, we compare our approach with other methods under both frame-level and video-level evaluations.

**Frame-level Evaluation.** Table 1 shows the cross-dataset evaluation results in frame-level AUC. The results for ED [1], CFM [28], and FIA-USA [30] are directly cited from the original paper and other results are cited from Forensics-Adapter [6] under DeepFakeBench [45]. Effort [47] do not report frame-level results, so we reproduce them using its open source code. From the table, we can observe that our approach outperforms the current state-of-the-art methods Effort and Forensics-Adapter. On the widely regarded most challenging DFDC and DFDCP datasets, our method surpasses Forensics-Adapter by 1% (from 0.843 to 0.853) and 1.5% (from 0.890 to 0.905) AUC respectively. These results demonstrate the excellent generalization performance of our method.

**Video-level Evaluation.** Table 2 shows the cross-dataset evaluation results in video-level AUC. We compare 10 state-

Method	Venue	CDF-v1	CDF-v2	DFDC	DFDCP	DFD	Avg.
Xception [5]	ICCV'19	0.779	0.737	0.708	0.737	0.816	0.755
F3Net [37]	ECCV'20	0.777	0.735	0.702	0.735	0.798	0.749
SPSL [26]	CVPR'21	0.815	0.765	0.704	0.741	0.812	0.767
SRM [29]	CVPR'21	0.793	0.755	0.700	0.741	0.812	0.760
Recce [3]	CVPR'22	0.768	0.732	0.713	0.734	0.812	0.752
UCF [44]	ICCV'23	0.779	0.753	0.719	0.759	0.807	0.763
ED [1]	AAAI'24	0.818	0.864	0.721	0.851	-	-
CFM [28]	TIFS'24	-	0.828	-	0.758	0.915	-
LSDA [46]	CVPR'24	0.867	0.830	0.736	0.815	0.880	0.826
UDD [11]	AAAI'25	-	0.869	0.758	0.856	0.910	-
FIA-USA [30]	arXiv'25	0.901	0.867	-	0.818	0.821	-
GM-DF [20]	ACM MM'25	0.893	0.892	<u>0.847</u>	0.882	0.928	0.888
Effort <sup>†</sup> [47]	ICML'25	<u>0.915</u>	0.898	0.825	0.860	<u>0.932</u>	0.886
Forensics-Adapter [6]	CVPR'25	0.914	<u>0.900</u>	0.843	<u>0.890</u>	<b>0.933</b>	0.896
SeLop (Ours)	-	<b>0.924</b>	<b>0.901</b>	<b>0.853</b>	<b>0.905</b>	0.926	<b>0.902</b>

Table 1. Cross-dataset evaluation results (**Frame-level AUC**). All methods are trained on FF++ and evaluated on other datasets. The **best** results are indicated in bold and the second-best results are underlined. “<sup>†</sup>” indicates that we reproduce results with its original code.

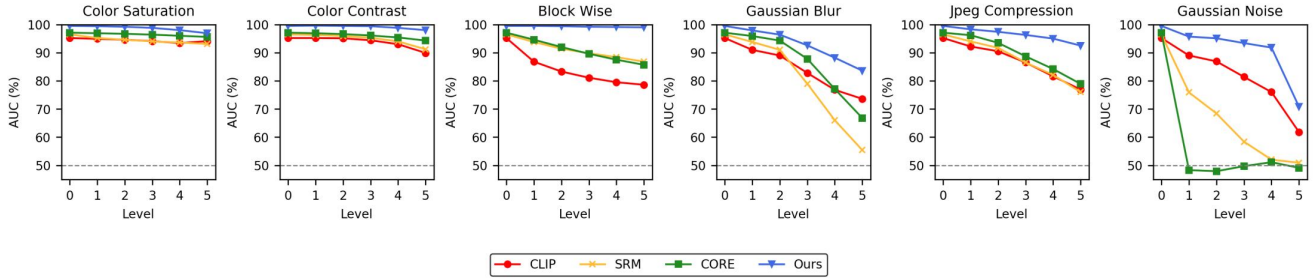


Figure 3. Robustness Analysis. Our method is compared with CLIP[38], SRM[29], and CORE[34] across five levels of six particular types of perturbations in **video-level AUC**.

Method	Venue	CDF-v2	DFDC	DFDCP
SBI [41]	CVPR'22	0.932	0.724	0.862
RealForensics [13]	CVPR'22	0.869	0.759	-
AUNet [2]	CVPR'23	0.928	0.738	0.862
SeeABLE [21]	ICCV'23	0.873	0.759	0.863
CADMM [10]	CVPR'23	0.939	0.739	-
IID [15]	CVPR'23	0.838	-	0.812
LAA-Net [33]	CVPR'24	<u>0.954</u>	-	0.869
TALL++ [43]	IJCV'24	0.920	0.785	-
MOE-FFD [18]	TDSC'25	0.913	-	0.850
Effort [47]	ICML'25	<b>0.956</b>	<u>0.843</u>	<u>0.909</u>
SeLop (Ours)	-	0.948	<b>0.877</b>	<b>0.929</b>

Table 2. Cross-dataset evaluation results (**Video-level AUC**). All the results are taken from their original papers.

of-the-art methods, with all results directly cited from their original papers. In video-level comparisons, our approach outperform the state-of-the-art Effort by 3.4% (from 0.843 to 0.877) and 2% (from 0.909 to 0.929) AUC on the DFDC

Method	Venue	CDF-v2	DFDC	DFDCP
Vanilla CLIP[38]	ICML'21	0.809	0.766	0.785
FFAA [16]	arXiv'24	-	0.740	-
MFCLIP [52]	TIFS'25	0.835	<u>0.861</u>	-
UDD [11]	AAAI'25	0.931	0.812	0.881
FCG [14]	CVPR'25	<b>0.950</b>	0.818	-
FFD-STA [49]	CVPR'25	0.947	0.843	<u>0.909</u>
SeLop (Ours)	-	<u>0.948</u>	<b>0.877</b>	<b>0.929</b>

Table 3. Cross-dataset evaluation results (**Video-level AUC**). Comparing our method with other CLIP-based methods.

and DFDCP datasets respectively, providing compelling evidence of its superior generalization.

**Compared with CLIP-based Methods.** Table 3 presents a comparison of our method with other CLIP-based methods. It can be observed that our method outperforms the second-best approach by 1.6% (from 0.861 to 0.877) and 2% (from 0.909 to 0.929) on the DFDC and DFDCP datasets respec-

Method	UniFace	BleFace	MobSwap	e4s	FaceDan	FSGAN	InSwap	SimSwap	Avg.
F3Net [37]	0.809	0.808	0.867	0.494	0.717	0.845	0.757	0.674	0.746
SPSL [26]	0.747	0.748	0.885	0.514	0.666	0.812	0.643	0.665	0.710
SRM [29]	0.749	0.704	0.779	0.704	0.659	0.772	0.793	0.694	0.732
SBI [41]	0.724	<u>0.891</u>	0.952	0.750	0.594	0.803	0.712	0.701	0.766
IID [15]	0.839	0.789	0.888	0.766	<u>0.844</u>	0.927	0.789	0.644	0.811
LSDA [46]	0.872	0.875	0.930	0.694	0.721	0.939	0.855	0.793	0.835
CDFa [25]	0.762	0.756	0.823	0.631	0.803	<u>0.942</u>	0.772	0.757	0.781
ProDet [4]	0.908	<b>0.929</b>	<b>0.975</b>	0.771	0.747	0.928	0.837	0.844	<u>0.867</u>
FIA-USA [30]	<u>0.918</u>	-	-	<u>0.875</u>	0.830	0.863	<u>0.874</u>	<b>0.910</b>	-
SeLop (Ours)	<b>0.925</b>	0.866	0.957	<b>0.940</b>	<b>0.880</b>	<b>0.952</b>	<b>0.897</b>	0.856	<b>0.909</b>

Table 4. Cross-manipulation evaluations within FF++ domain. All models are trained on FF++ (c23) and tested on the latest DF40[48] dataset. The best results are indicated in bold and the second-best results are underlined.

ID	SP	CA	CDF-v1			CDF-v2			DFDC			DFDCP			DFD		
			AUC $\uparrow$	AP $\uparrow$	EER $\downarrow$	AUC $\uparrow$	AP $\uparrow$	EER $\downarrow$	AUC $\uparrow$	AP $\uparrow$	EER $\downarrow$	AUC $\uparrow$	AP $\uparrow$	EER $\downarrow$	AUC $\uparrow$	AP $\uparrow$	EER $\downarrow$
1	✓	✓	0.781	0.859	0.299	0.763	0.862	0.309	0.742	0.770	0.326	0.761	0.869	0.316	0.828	0.978	0.248
2	✓	✗	0.543	0.645	0.455	0.544	0.699	0.475	0.661	0.690	0.385	0.611	0.720	0.416	0.619	0.928	0.417
3	✗	✓	<b>0.924</b>	<b>0.954</b>	<b>0.160</b>	<b>0.901</b>	<b>0.947</b>	<b>0.189</b>	<b>0.853</b>	<b>0.883</b>	<b>0.233</b>	<b>0.905</b>	<b>0.951</b>	<b>0.173</b>	<b>0.926</b>	<b>0.991</b>	<b>0.149</b>

Table 5. Ablation study on visual space intervention. Evaluation metrics are the frame-level AUC, AP, and EER, respectively.

tively. It is noteworthy that our approach significantly outperforms UDD, which specifically distinguishes and addresses one particular type of spurious correlation. The results further demonstrate the effectiveness of our approach.

**Cross-manipulation Evaluation.** Table 4 shows cross-manipulation evaluation results within FF++ domain. All models in the table were trained on the FF++ dataset and then tested on the DF40 [48] dataset. Note that DF40 includes multiple manipulation techniques (e.g., face swapping, face reenactment). It can be observed that our method achieves excellent detection performance when confronted with different manipulation techniques. In particular, our method outperforms the second-best method by 6.5% (from 0.875 to 0.940) and 3.6% (from 0.844 to 0.880) on the e4s [27] and FaceDancer [39] datasets, respectively.

**Robustness Evaluation.** Figure 3 shows robustness evaluation results. Similar to the settings in [11], we conduct robustness evaluation experiments using the FF++ test set. We employ the same configuration as in [17], including six different types of perturbations across five severity levels: color saturation, color contrast, block-wise, gaussian blur, JPEG compression, and gaussian noise. We compare our method with vanilla CLIP [38], SRM [29], and CORE [34]. It is evident that our method exhibits greater robustness. These methods are highly sensitive to perturbation-related information, being significantly susceptible to them. However, our method can truly focus on forgery-related features after eliminating spurious correlations, and is less susceptible to irrelevant noise.

### 5.3. Ablation Study

**Effectiveness of LROR.** To verify that our method can project spurious correlations into a low-rank subspace and remove them from the original representation, we conduct a counterfactual validation experiment. Quantitative and qualitative experiments are shown in Table 5 and Figure 4. We replace the forward visual space with two complementary forms for comparative validation. The first is the non-causal factor space  $\mathbf{X}_{\text{vis}} \mathbf{Q} \mathbf{Q}^\top$  (denoted by SP, representing the subspace of spurious correlations). We achieve this setting by fixing  $\mathbf{Q}$  obtained from trained SeLop, replacing only the forward flow with  $\mathbf{X}_{\text{vis}} \mathbf{Q} \mathbf{Q}^\top$ , and retraining the linear classification head. The second is the causal factor space  $\mathbf{X}_{\text{vis}} (\mathbf{I} - \mathbf{Q} \mathbf{Q}^\top)$  (denoted by CA, representing the visual space after our method’s intervention). ID1 in Table 5 is the Vanilla CLIP, without subspace replacement or intervention, where forgery-related knowledge is intertwined with irrelevant factors to forgery. As can be seen in Figure 4 (a), the distributions of real and forged samples overlap significantly, making it difficult to form a robust decision boundary. When the visual space consists solely of non-causal factors (corresponding to ID2 and Figure 4 (b)), the AUC performance across several datasets hovers around 0.5, with lower AP and higher error rate. This near-random performance suggests that this subspace primarily contains non-causal features, making it difficult for the model to accurately distinguish real from fake faces based on this information. However, after intervention with our method (corresponding to ID3 and Figure 4 (c)), the AUC and AP

rank	layers	CDF-v2			DFDC			DFD			MobSwap			BleFace		
		AUC $\uparrow$	AP $\uparrow$	EER $\downarrow$	AUC $\uparrow$	AP $\uparrow$	EER $\downarrow$	AUC $\uparrow$	AP $\uparrow$	EER $\downarrow$	AUC $\uparrow$	AP $\uparrow$	EER $\downarrow$	AUC $\uparrow$	AP $\uparrow$	EER $\downarrow$
28	8	0.845	0.915	0.239	0.836	0.869	0.244	0.898	0.987	0.173	0.851	0.972	0.230	0.770	0.777	0.306
32	8	0.858	0.922	0.230	0.842	0.868	0.237	0.917	0.990	0.154	0.877	0.977	0.205	0.764	0.773	0.309
36	8	0.891	0.940	0.197	0.840	0.873	0.242	0.918	0.990	0.152	0.878	0.976	0.200	0.789	0.791	0.291
28	12	0.883	0.936	0.198	<b>0.868</b>	<b>0.899</b>	<b>0.209</b>	0.918	0.990	0.152	0.896	0.981	0.188	0.771	0.785	0.304
32	12	<b>0.901</b>	<b>0.947</b>	<b>0.187</b>	<b>0.853</b>	<b>0.883</b>	<b>0.233</b>	<b>0.926</b>	<b>0.991</b>	<b>0.149</b>	<b>0.913</b>	<b>0.984</b>	<b>0.163</b>	<b>0.807</b>	<b>0.818</b>	<b>0.265</b>
36	12	<b>0.901</b>	<b>0.947</b>	<b>0.187</b>	0.838	0.865	0.242	<b>0.932</b>	<b>0.992</b>	<b>0.142</b>	0.870	0.975	0.206	<b>0.790</b>	<b>0.797</b>	<b>0.274</b>
28	16	<b>0.896</b>	<b>0.943</b>	<b>0.189</b>	0.839	0.865	0.247	0.915	0.989	0.163	<b>0.894</b>	<b>0.980</b>	<b>0.179</b>	0.775	0.784	0.289
32	16	0.858	0.928	0.216	0.813	0.846	0.261	0.884	0.985	0.186	0.862	0.973	0.214	0.783	0.783	0.292
36	16	0.819	0.883	0.258	0.713	0.757	0.352	0.849	0.978	0.234	0.754	0.942	0.316	0.709	0.710	0.351

Table 6. Ablation study on rank of spurious correlation subspace and number of intervention layers. Evaluation metrics are the frame-level AUC, AP, and EER, respectively.

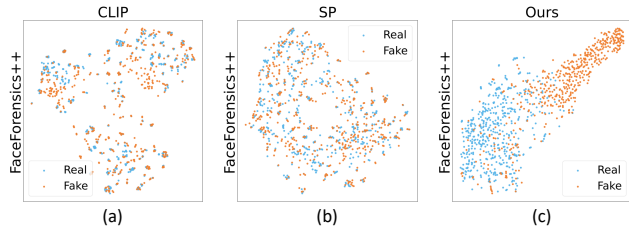


Figure 4. T-SNE Visualizations. The feature distribution before and after intervention in visual space of CLIP[38]: Vanilla CLIP (left, before intervention), spurious correlation subspace (mid), our method (right, after intervention).

on each benchmark significantly improve, the EER significantly decreases, and T-SNE visualizations [31] demonstrate clear between-class separation. This demonstrates that our method effectively removes the low-rank spurious correlation subspace induced by confounding factors at the representation level and focuses the spurious correlation factors on orthogonal complements, resulting in consistent improvements across datasets.

**Impact of Different Hyperparameters.** In this section, we investigate the impact of different ranks of the low-rank subspace and numbers of intervention layers on detection performance of our model. As shown in the Table 6, we can observe that: (1) For the rank of the spurious correlation space, if rank is too small, it fails to eliminate most spurious correlation factors, and if rank is too large, it may hinder the sufficient learning of forgery-related features. (2) Regarding the number of intervention layers, fewer intervention cannot completely decouple spurious correlation in the visual space and excessive intervention may destroy pre-trained knowledge of the CLIP [38]. Therefore, we select rank=32 and layers=12 as the hyperparameters for the model in this paper.

**Complexity Analysis.** In this section, we examine the computational complexity of our approach. By freezing all parameters of CLIP and only training the low-rank orthogonal space for visual intervention alongside a linear classifica-

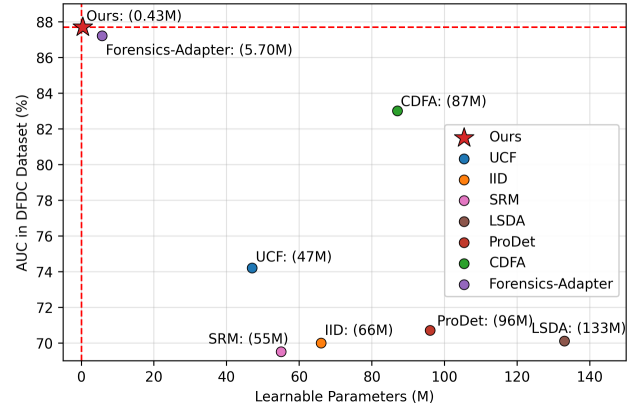


Figure 5. Comparison between our method and other SOTA detectors on the DFDC dataset (trained on FF++). Our method needs the fewest learnable parameters while achieves the best performance.

tion head, our model requires a mere **0.43 million** trainable parameters. Compared to methods employing adapters for fine-tuning, our approach is remarkably lightweight. As demonstrated in Figure 5, our approach achieves the best performance with the fewest trainable parameters, thereby proving its superiority.

## 6. Conclusion

In this paper, we analyze the reasons of failures of Vanilla CLIP’s generalization from the perspective of causal learning. Unlike previous approaches that identify specific spurious correlation and then design specialised modules to mitigate their effects, we treat spurious correlations as a collective phenomenon. Specifically, we intervene in CLIP’s visual representation space by removing spurious correlation subspaces through orthogonal low-rank projection, compelling the model to implement classification based on real causal factors (e.g., forgery-related features). Qualitative and quantitative analysis demonstrated its effectiveness. Extensive experiments on several benchmarks demonstrate our approach’s outstanding generalization and robustness.

## References

[1] Zhongjie Ba, Qingyu Liu, Zhenguang Liu, Shuang Wu, Feng Lin, Li Lu, and Kui Ren. Exposing the deception: Uncovering more forgery clues for deepfake detection. In *Proceedings of the AAAI Conference on Artificial Intelligence*, pages 719–728, 2024. 5, 6

[2] Weiming Bai, Yufan Liu, Zhipeng Zhang, Bing Li, and Weiming Hu. Aunet: Learning relations between action units for face forgery detection. In *Proceedings of the IEEE/CVF conference on computer vision and pattern recognition*, pages 24709–24719, 2023. 6

[3] Junyi Cao, Chao Ma, Taiping Yao, Shen Chen, Shouhong Ding, and Xiaokang Yang. End-to-end reconstruction-classification learning for face forgery detection. In *Proceedings of the IEEE/CVF conference on computer vision and pattern recognition*, pages 4113–4122, 2022. 6

[4] Jikang Cheng, Zhiyuan Yan, Ying Zhang, Yuhao Luo, Zhongyuan Wang, and Chen Li. Can we leave deepfake data behind in training deepfake detector? *Advances in Neural Information Processing Systems*, 37:21979–21998, 2024. 7

[5] François Chollet. Xception: Deep learning with depthwise separable convolutions. In *Proceedings of the IEEE conference on computer vision and pattern recognition*, pages 1251–1258, 2017. 6

[6] Jinjie Cui, Yuezun Li, Ao Luo, Jiaran Zhou, and Junyu Dong. Forensics adapter: Adapting clip for generalizable face forgery detection. In *Proceedings of the Computer Vision and Pattern Recognition Conference*, pages 19207–19217, 2025. 2, 3, 5, 6

[7] Deepfakedetection. <https://ai.googleblog.com/2019/09/contributing-data-to-deepfake-detection.html>, 2019. Accessed: 2021-11-13. 5

[8] B Dolhansky, R Howes, B Pflaum, N Baram, and CC Ferrer. The deepfake detection challenge (dfdc) preview dataset. arxiv 2019. *arXiv preprint arXiv:1910.08854*, 2019. 5

[9] Brian Dolhansky, Joanna Bitton, Ben Pflaum, Jikuo Lu, Russ Howes, Menglin Wang, and Cristian Canton Ferrer. The deepfake detection challenge (dfdc) dataset. *arXiv preprint arXiv:2006.07397*, 2020. 5

[10] Shichao Dong, Jin Wang, Renhe Ji, Jiajun Liang, Haoqiang Fan, and Zheng Ge. Implicit identity leakage: The stumbling block to improving deepfake detection generalization. In *Proceedings of the IEEE/CVF Conference on Computer Vision and Pattern Recognition*, pages 3994–4004, 2023. 2, 6

[11] Xinghe Fu, Zhiyuan Yan, Taiping Yao, Shen Chen, and Xi Li. Exploring unbiased deepfake detection via token-level shuffling and mixing. In *Proceedings of the AAAI Conference on Artificial Intelligence*, pages 3040–3048, 2025. 3, 5, 6, 7

[12] Alexandros Haliassos, Konstantinos Vougioukas, Stavros Petridis, and Maja Pantic. Lips don’t lie: A generalisable and robust approach to face forgery detection. In *Proceedings of the IEEE/CVF conference on computer vision and pattern recognition*, pages 5039–5049, 2021. 2

[13] Alexandros Haliassos, Rodrigo Mira, Stavros Petridis, and Maja Pantic. Leveraging real talking faces via self-supervision for robust forgery detection. In *Proceedings of the IEEE/CVF conference on computer vision and pattern recognition*, pages 14950–14962, 2022. 6

[14] Yue-Hua Han, Tai-Ming Huang, Kai-Lung Hua, and Jun-Cheng Chen. Towards more general video-based deepfake detection through facial component guided adaptation for foundation model. In *Proceedings of the Computer Vision and Pattern Recognition Conference*, pages 22995–23005, 2025. 2, 6

[15] Baojin Huang, Zhongyuan Wang, Jifan Yang, Jiaxin Ai, Qin Zou, Qian Wang, and Dengpan Ye. Implicit identity driven deepfake face swapping detection. In *Proceedings of the IEEE/CVF conference on computer vision and pattern recognition*, pages 4490–4499, 2023. 6, 7

[16] Zhengchao Huang, Bin Xia, Zicheng Lin, Zhun Mou, Weming Yang, and Jiaya Jia. Ffaa: Multimodal large language model based explainable open-world face forgery analysis assistant. *arXiv preprint arXiv:2408.10072*, 2024. 6

[17] Liming Jiang, Ren Li, Wayne Wu, Chen Qian, and Chen Change Loy. Deeperforensics-1.0: A large-scale dataset for real-world face forgery detection. In *Proceedings of the IEEE/CVF conference on computer vision and pattern recognition*, pages 2889–2898, 2020. 7

[18] Chenqi Kong, Anwei Luo, Peijun Bao, Yi Yu, Haoliang Li, Zengwei Zheng, Shiqi Wang, and Alex C Kot. Moe-ffd: Mixture of experts for generalized and parameter-efficient face forgery detection. *IEEE Transactions on Dependable and Secure Computing*, 2025. 2, 6

[19] Marek Kowalski. Faceswap. <https://github.com/deepfakes/faceswap>, 2019. 1

[20] Yingxin Lai, Zitong Yu, Jing Yang, Bin Li, Xiangui Kang, and Linlin Shen. Gm-df: Generalized multi-scenario deepfake detection. *arXiv preprint arXiv:2406.20078*, 2024. 3, 6

[21] Nicolas Larue, Ngoc-Son Vu, Vitomir Struc, Peter Peer, and Vassilis Christophides. Seeable: Soft discrepancies and bounded contrastive learning for exposing deepfakes. In *Proceedings of the IEEE/CVF International Conference on Computer Vision*, pages 21011–21021, 2023. 6

[22] Lingzhi Li, Jianmin Bao, Ting Zhang, Hao Yang, Dong Chen, Fang Wen, and Baining Guo. Face x-ray for more general face forgery detection. In *Proceedings of the IEEE/CVF conference on computer vision and pattern recognition*, pages 5001–5010, 2020. 3

[23] Yuezun Li, Xin Yang, Pu Sun, Honggang Qi, and Siwei Lyu. Celeb-df: A large-scale challenging dataset for deepfake forensics. In *Proceedings of the IEEE/CVF conference on computer vision and pattern recognition*, pages 3207–3216, 2020. 5

[24] Kaiqing Lin, Yuzhen Lin, Weixiang Li, Taiping Yao, and Bin Li. Standing on the shoulders of giants: Reprogramming visual-language model for general deepfake detection. In *Proceedings of the AAAI Conference on Artificial Intelligence*, pages 5262–5270, 2025. 2, 3

[25] Yuzhen Lin, Wentang Song, Bin Li, Yuezun Li, Jiangqun Ni, Han Chen, and Qiushi Li. Fake it till you make it: Curricular dynamic forgery augmentations towards general deep

fake detection. In *European Conference on Computer Vision*, pages 104–122. Springer, 2024. 7

[26] Honggu Liu, Xiaodan Li, Wenbo Zhou, Yuefeng Chen, Yuan He, Hui Xue, Weiming Zhang, and Nenghai Yu. Spatial-phase shallow learning: rethinking face forgery detection in frequency domain. In *Proceedings of the IEEE/CVF conference on computer vision and pattern recognition*, pages 772–781, 2021. 6, 7

[27] Zhan Liu, Maomao Li, Yong Zhang, Cairong Wang, Qi Zhang, Jue Wang, and Yongwei Nie. Fine-grained face swapping via regional gan inversion. In *Proceedings of the IEEE/CVF conference on computer vision and pattern recognition*, pages 8578–8587, 2023. 7

[28] Anwei Luo, Chenqi Kong, Jiwu Huang, Yongjian Hu, Xian-gui Kang, and Alex C Kot. Beyond the prior forgery knowledge: Mining critical clues for general face forgery detection. *IEEE Transactions on Information Forensics and Security*, 19:1168–1182, 2023. 5, 6

[29] Yuchen Luo, Yong Zhang, Junchi Yan, and Wei Liu. Generalizing face forgery detection with high-frequency features. In *Proceedings of the IEEE/CVF conference on computer vision and pattern recognition*, pages 16317–16326, 2021. 6, 7

[30] Long Ma, Zhiyuan Yan, Yize Chen, Jin Xu, Qinglang Guo, Hu Huang, Yong Liao, and Hui Lin. From specificity to generality: Revisiting generalizable artifacts in detecting face deepfakes. *arXiv preprint arXiv:2504.04827*, 2025. 5, 6, 7

[31] Laurens van der Maaten and Geoffrey Hinton. Visualizing data using t-sne. *Journal of machine learning research*, 9 (Nov):2579–2605, 2008. 8

[32] Changtao Miao, Zichang Tan, Qi Chu, Huan Liu, Honggang Hu, and Nenghai Yu. F 2 trans: High-frequency fine-grained transformer for face forgery detection. *IEEE Transactions on Information Forensics and Security*, 18:1039–1051, 2023. 2

[33] Dat Nguyen, Nesryne Mejri, Inder Pal Singh, Polina Kuleshova, Marcella Astrid, Anis Kacem, Enjie Ghorbel, and Djamilia Aouada. Laa-net: Localized artifact attention network for quality-agnostic and generalizable deepfake detection. In *Proceedings of the IEEE/CVF Conference on Computer Vision and Pattern Recognition*, pages 17395–17405, 2024. 6

[34] Yunsheng Ni, Depu Meng, Changqian Yu, Chengbin Quan, Dongchun Ren, and Youjian Zhao. Core: Consistent representation learning for face forgery detection. In *Proceedings of the IEEE/CVF conference on computer vision and pattern recognition*, pages 12–21, 2022. 6, 7

[35] Judea Pearl. *Causality*. Cambridge university press, 2009. 3

[36] Chunlei Peng, Zimin Miao, Decheng Liu, Nannan Wang, Ruimin Hu, and Xinbo Gao. Where deepfakes gaze at? spatial-temporal gaze inconsistency analysis for video face forgery detection. *IEEE Transactions on Information Forensics and Security*, 2024. 2

[37] Yuyang Qian, Guojun Yin, Lu Sheng, Zixuan Chen, and Jing Shao. Thinking in frequency: Face forgery detection by mining frequency-aware clues. In *European conference on computer vision*, pages 86–103. Springer, 2020. 2, 6, 7

[38] Alec Radford, Jong Wook Kim, Chris Hallacy, Aditya Ramesh, Gabriel Goh, Sandhini Agarwal, Girish Sastry, Amanda Askell, Pamela Mishkin, Jack Clark, et al. Learning transferable visual models from natural language supervision. In *International conference on machine learning*, pages 8748–8763. PMLR, 2021. 1, 2, 3, 6, 7, 8

[39] Felix Rosberg, Eren Erdal Aksoy, Fernando Alonso-Fernandez, and Cristofer Englund. Facedancer: Pose-and occlusion-aware high fidelity face swapping. In *Proceedings of the IEEE/CVF winter conference on applications of computer vision*, pages 3454–3463, 2023. 7

[40] Andreas Rossler, Davide Cozzolino, Luisa Verdoliva, Christian Riess, Justus Thies, and Matthias Nießner. Faceforensics++: Learning to detect manipulated facial images. In *Proceedings of the IEEE/CVF international conference on computer vision*, pages 1–11, 2019. 5

[41] Kaede Shiohara and Toshihiko Yamasaki. Detecting deepfakes with self-blended images. In *Proceedings of the IEEE/CVF conference on computer vision and pattern recognition*, pages 18720–18729, 2022. 2, 3, 6, 7

[42] Qingzhong Wang, Pengfei Zhang, Haoyi Xiong, and Jian Zhao. Face. evolve: A high-performance face recognition library. *arXiv preprint arXiv:2107.08621*, 2021. 1

[43] Yuting Xu, Jian Liang, Lijun Sheng, and Xiao-Yu Zhang. Learning spatiotemporal inconsistency via thumbnail layout for face deepfake detection. *International Journal of Computer Vision*, 132(12):5663–5680, 2024. 6

[44] Zhiyuan Yan, Yong Zhang, Yanbo Fan, and Baoyuan Wu. Ucf: Uncovering common features for generalizable deepfake detection. In *Proceedings of the IEEE/CVF International Conference on Computer Vision*, pages 22412–22423, 2023. 6

[45] Zhiyuan Yan, Yong Zhang, Xinhang Yuan, Siwei Lyu, and Baoyuan Wu. Deepfakebench: A comprehensive benchmark of deepfake detection. *arXiv preprint arXiv:2307.01426*, 2023. 5

[46] Zhiyuan Yan, Yuhao Luo, Siwei Lyu, Qingshan Liu, and Baoyuan Wu. Transcending forgery specificity with latent space augmentation for generalizable deepfake detection. In *Proceedings of the IEEE/CVF Conference on Computer Vision and Pattern Recognition*, pages 8984–8994, 2024. 5, 6, 7

[47] Zhiyuan Yan, Jiangming Wang, Peng Jin, Ke-Yue Zhang, Chengchun Liu, Shen Chen, Taiping Yao, Shouhong Ding, Baoyuan Wu, and Li Yuan. Orthogonal subspace decomposition for generalizable ai-generated image detection. *arXiv preprint arXiv:2411.15633*, 2024. 2, 3, 5, 6

[48] Zhiyuan Yan, Taiping Yao, Shen Chen, Yandan Zhao, Xinghe Fu, Junwei Zhu, Donghao Luo, Chengjie Wang, Shouhong Ding, Yunsheng Wu, et al. Df40: Toward next-generation deepfake detection. *arXiv preprint arXiv:2406.13495*, 2024. 5, 7

[49] Zhiyuan Yan, Yandan Zhao, Shen Chen, Mingyi Guo, Xinghe Fu, Taiping Yao, Shouhong Ding, Yunsheng Wu, and Li Yuan. Generalizing deepfake video detection with plug-and-play: Video-level blending and spatiotemporal adapter tuning. In *Proceedings of the Computer Vision and Pattern Recognition Conference*, pages 12615–12625, 2025. 5, 6

[50] Liuyi Yao, Sheng Li, Yaliang Li, Mengdi Huai, Jing Gao, and Aidong Zhang. Representation learning for treatment

effect estimation from observational data. *Advances in neural information processing systems*, 31, 2018. 3

[51] Pengfei Yue, Beijing Chen, and Zhangjie Fu. Local region frequency guided dynamic inconsistency network for deepfake video detection. *Big Data Mining and Analytics*, 7(3):889–904, 2024. 1

[52] Yaning Zhang, Tianyi Wang, Zitong Yu, Zan Gao, Linlin Shen, and Shengyong Chen. Mfclip: Multi-modal fine-grained clip for generalizable diffusion face forgery detection. *IEEE Transactions on Information Forensics and Security*, 2025. 2, 6

[53] Qihua Zhou, Zhili Zhou, Zhipeng Bao, Weinan Niu, and Yuling Liu. Iin-ffd: intra-inter network for face forgery detection. *Tsinghua Science and Technology*, 29(6):1839–1850, 2024. 1